Astron. Astrophys. 325, 484–492 (1997)

ASTRONOMY
AND
ASTROPHYSICS

The parsec-scale evolution of the superluminal quasar 1642+690

T. Venturi[1,2], **T.J. Pearson**[2], **P.D. Barthel**[3], **and S.C. Unwin**[2,4]

[1] Istituto di Radioastronomia del CNR, Via Gobetti 101, I-40129, Bologna, Italy
[2] California Institute of Technology, 105-24, Pasadena, CA 91125, USA
[3] Kapteyn Astronomical Institute, P. O. Box 800, AV Groningen, The Netherlands
[4] Jet Propulsion Laboratory, 4800 Oak Grove Drive, Pasadena, CA 91109-8099, USA

Received 24 February 1997 / Accepted 21 March 1997

Abstract. We present the results of a 6 cm VLBI monitoring program of the core dominated, radio loud quasar 1642+690. 3.6 cm VLBI observations are also presented. The 6 cm observations, carried out in 1986.4, 1988.2, 1992.2 and 1994.7 confirm that the source is variable, both in morphology and in flux density, its changes reflecting a complicated evolution.

We propose a few evolutionary scenarios, and favour the interpretation of the superluminal character of 1642+690, with a flow of superluminal components ejected from the core at a very similar high apparent speed, $\beta_{\rm app} \sim 9$, in agreement with the first claim of superluminal motion in this source.

Key words: galaxies: active – quasars: general – radio continuum: galaxies – quasars: Q1642+690

1. Introduction

The radio source 1642+690 is associated with a 19th magnitude quasar at z = 0.751. At radio frequencies, 1642+690 is dominated by a strong compact core, with faint emission in the shape of a bent jet. The jet extends out to $\sim 4''$ in position angle $\sim 180^\circ$ close to the core and $\sim 170^\circ$ further out (O'Dea et al. 1988 and references therein). Radio emission is also present on the counterjet side, at $6''$ from the core in position angle $\sim 12^\circ$. High dynamic range VLA observations at 1.65 GHz (Murphy et al. 1993) revealed that the 10 arcsecond triple source is surrounded by a low brightness halo. The large scale radio emission is polarised by a few percent, both in the core and along the jet (Wrobel 1993).

The compact radio core was observed with the VLBI technique at 6 cm as part of the Pearson and Readhead survey (Pearson & Readhead 1988, and references therein). The source was reported to be superluminal by Pearson et al. (1986, hereafter Paper I), and the strong morphological changes in the parsec-scale structure were interpreted as due to Doppler boosting in a source aligned to the line of sight, and the superluminal motion detected for one of the components in the source was discussed within this theoretical frame (Pearson & Zensus 1987). The apparent velocity derived for 1642+690 on the basis of the first two epochs was one of the highest ever detected, i.e. $v_{\rm app}$ = 9.3c (H_0 = 100 km s^{-1}Mpc^{-1}, q_0 = 0.05). The difference in position angle between the parsec and kiloparsec scale in 1642+690 is roughly 20°, i.e., this source is considered almost aligned according to the bimodal distribution of misalignment angles between the parsec and kiloparsec-scale jets in powerful radio sources (Pearson & Readhead 1988; Conway & Murphy 1993). No information on its VLBI polarisation is available.

1642+690 was observed with the Energetic Gamma Ray Experiment Telescope (EGRET) in the energy range $\sim 3 \times 10^7 - 10^{10}$ eV, and only an upper limit to its flux density was obtained from the observations (Fichtel et al. 1994).

We observed 1642+690 four times in the time interval 1986−1994, at 6 cm at VLBI resolution, in order to follow the changes of the parsec-scale morphology and the motion of the superluminal component. We carried out also 3.6 cm VLBI observations (epoch 1991.9) in order to better resolve the parsec-scale jet and to compute the spectral index of the VLBI structure. In this paper we will present and discuss the results of our monitoring program and of the VLBI observations made at 3.6 cm.

We will assume $S \propto \nu^{-\alpha}$ and will use a Hubble constant H_0 = 100 km s^{-1}Mpc^{-1} and a deceleration parameter q_0 = 0.05 throughout the paper. At the redshift of the quasar, our choice of the cosmological parameters gives 1 mas = 4.8 pc, and a proper motion μ = 1 mas yr^{-1} corresponds to $\beta_{\rm app}$ = 27.3.

2. Observations and data reduction

2.1. The monitoring at 6 cm

1642+690 was observed at 6 cm (ν_{obs} = 4990.99 MHz) with the global VLBI array (European VLBI Network and US Network) at four epochs: 1986.4, 1988.2, 1992.2 and 1994.7. The source was observed in a full track mode during the first three epochs, while in 1994.7 a snap-shot mode observing strategy was followed (see Polatidis et al. 1995). The signal was recorded with the MK2 recording mode, with a 2 MHz bandwidth, and the data were correlated with the Caltech/JPL Block 2 Correlator

Table 1. VLBI observations

(1) ν MHz	(2) Epoch	(3) Obs. Time hr	(4) Array	(5) u-v coverage Mλ
4990.99	1986.4	12	EU - US[a]	4 - 145
	1988.2	8	EU-US[b]	10 - 126
	1992.2	6	EU,US,VLBA[c]	2 - 152
	1994.7	2	EU,US,VLBA[d]	3 - 180
8416.99	1991.9	7	EU,US,VLBA[e]	2 - 264

B=Bonn, W=Westerbork Synthesis Radio Telescope, S=Onsala, J=Jodrell Bank, L=Medicina, N=Noto, K=Haystack, G=Green Bank, F=Iowa, Y=Very Large Array, single antenna, O=Owens Valley, Ht=Hartebeesthoek

[a] EU = BWSJL, US = KGFYOHt

[b] EU = BWSJL, US = KGYIO

[c] EU = BWSJLN, US = KGY, VLBA = Kp,Pt,La,Fd,Br,Ov

[d] EU = WSL, US = GY, VLBA = Pt,Nl,Ov,Mk,Br,Sc,Hn

[e] EU = BLN, US = KGY, VLBA = Kp,Pt,La,Fd,Nl,Ov

at the California Institute of Technology. In Table 1 we give the total observing time (col. 3), the array for each epoch (col. 4), the shortest and longest baseline in the u-v coverage (col. 5).

During the first three epochs the source 1739+522 was used as calibrator and 3C345 as fringe finder. We followed the same data reduction strategy for each of these three datasets. The correlated raw data were corrected for residual delay and fringe-rate, using the AIPS task FRING (Schwab & Cotton 1983), then the data reduction was carried out using the Caltech Package (Pearson 1991). After amplitude calibration and editing of bad points, the data were modelfitted with a simple model consisting of gaussian components. The best model obtained from modelfitting was then used as input model for phase self-calibration and hybrid mapping. When the phases were stable, phase and gain self-calibration were applied for two cycles. Amplitude corrections were $\leq 5\%$ for each dataset. With this starting method, convergence between the observed visibility and the model was reached after a small number (from 7 to 9, depending on the epoch) of self-calibration and mapping iterations.

The data reduction method applied to the 1994.7 dataset was the same as described by Polatidis et al. (1995) and Taylor et al. (1994). After fringe fitting and amplitude calibration, the data were self-calibrated, starting with a point source model, by means of the package DIFMAP (Shepherd et al. 1994). Final convergence between the data and the source model was reached after several iterations of self-calibration and mapping.

Contour plots of the final maps at 6 cm are given in Fig. 1a–d. In Table 2 details on the maps are given: epoch of the observations (col. 1), restoring beam (col. 2), noise in the final map (col. 3), total VLBI flux density (col. 4), flux density in the VLBI core (col. 5), flux density of the southernmost component K (col. 6) and SNR (col. 7), computed by comparing the peak in the map to the r.m.s measured in a region far from the source. In spite of the fact that the telescopes taking part to the observations and the observing strategy changed from 1986.4 to 1994.7, the numbers given in Table 2 indicate that the quality of the four 6 cm maps is comparable.

2.2. The 3.6 cm observations

The source was observed at 3.6 cm (ν = 8416.99 MHz) in November 1991 for 7 hours with the global VLBI array, and the data were recorded with the MK2 recording system. Details on the observation are given in Table 1. The data were correlated with the Block 2 Correlator at the California Institute of Technolgy and the data reduction was carried out as described in *Sect. 2.1*. The final full resolution map is shown in Fig. 2, and the observational parameters of the map are given in Table 2.

3. Results

On the VLBI scale 1642+690 is characterised by a one-sided jet-like morphology, aligned roughly in p.a. 194°. The northernmost component (Figs. 1a–d) is the most compact and is unresolved in our maps at both 6 cm and 3.6 cm; furthermore, it has an inverted spectrum between 3.6 cm and 6 cm, as discussed in detail in Sect. 3.3. For these two reasons we consider it to be the core of the radio emission. In order to classify the source morphology and to interpret our results, we will assume that the 1642+690 core is a stationary feature.

3.1. The monitoring at 6 cm

The overall structure of the source, such as the jet direction and the presence of knots along the jet, is similar in the four 6 cm maps and in the 3.6 cm map; however, a careful inspection of the various features reveals that 1642+690 changed considerably from 1986.4 to 1994.7. The total extension of the source increased from $\sim$ 6.7 mas in 1986.4 to almost 10 mas in 1994.7. Furthermore the morphology of the various components along the jet is clearly variable. These changes are even more striking if we also take into account the source structure in the first two epochs (see Paper I). For a straightforward comparison of the morphologies, all six maps, convolved with the same 1 mas (HPBW) circular beam, are shown in Fig. 3. The contour plots show regions of equal brightness at each epoch.

In order to make sure that the maps taken at the earlier epochs are comparable to those presented in this paper, and that no outer components were missed as a consequence of the poorer u-v coverage of the older data sets (Paper I), we remapped the last four epochs using only the five stations forming the array in the first two epochs, obtaining a comparable u-v coverage. The four resulting maps, not presented here, have a sensitivity and dynamic range comparable to those of the first and second epoch maps. Even with limited u-v coverage, the maps contain all features in the source, from the nuclear region to the outermost component.

Inspection of Fig. 3 suggests that major changes took place in the overall structure of 1642+690 during our fifteen years of monitoring. Between 1983.9 and 1986.4 the morphology of the southermost component changed completely. The innermost region changed completely between 1992.2 and 1994.7: the core flux decreased dramatically while the position angle of the component closest to the core rotated by $\sim$ 15° and its flux increased

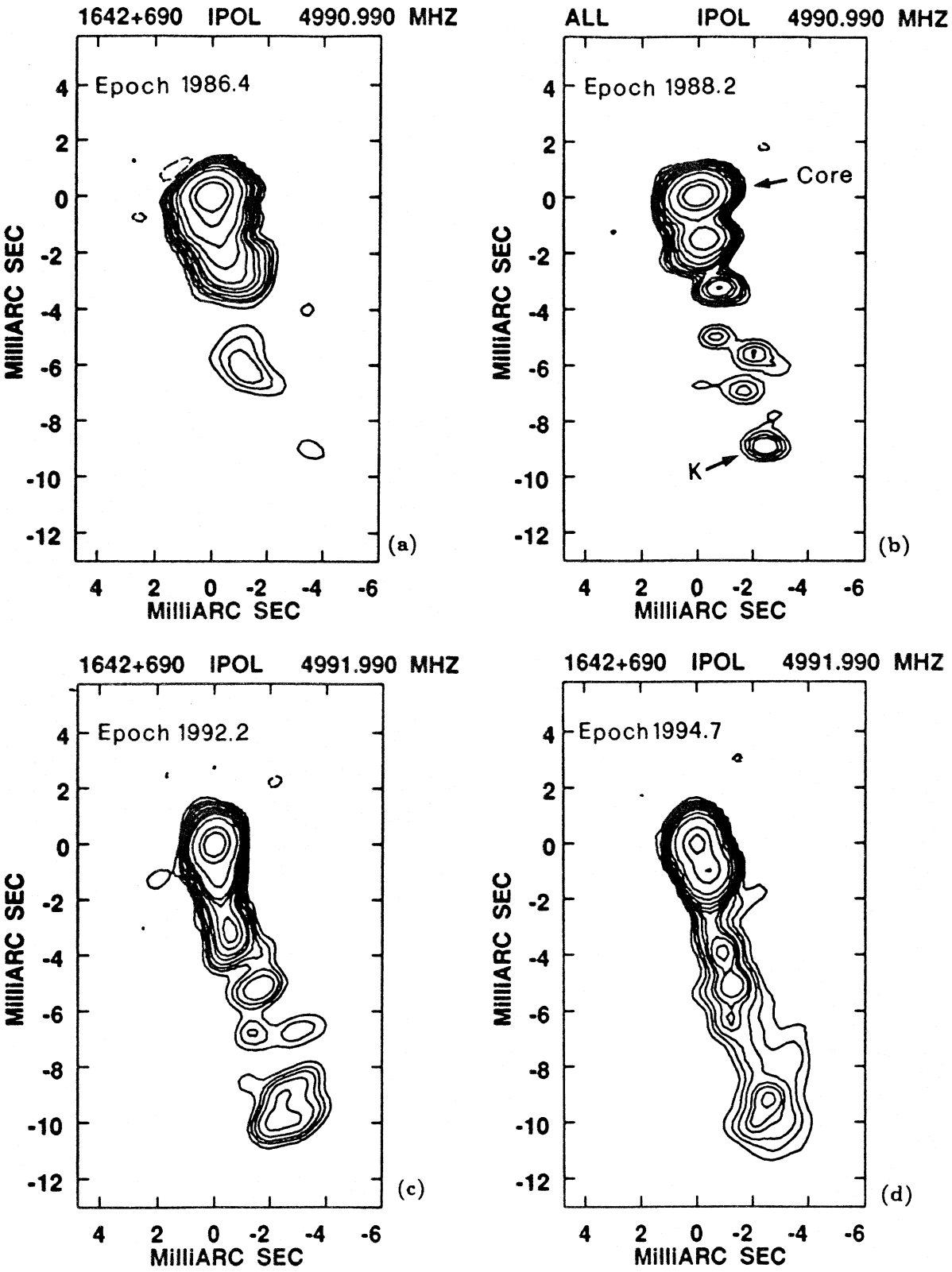

Fig. 1a–d. Contour plots of the 6 cm maps. **a** Epoch 1986.4. Peak flux is 953.7 mJy/beam. Levels are −3, 3, 5, 7, 10, 15, 20, 30, 50, 100, 300, 500 mJy/beam. The HPBW of the restoring beam is 1.16×0.67, p.a. −82°. **b** Epoch 1988.2. Peak flux is 916 mJy/beam. Levels are -4, 4, 6, 8, 10, 15, 20, 30, 50, 100, 300, 500 mJy/beam. The HPBW of the restoring beam is 1.16×0.67, p.a. -82°. **c** Epoch 1992.2. Peak flux is 835.9 mJy/beam. Levels are −3, 3, 5, 7, 10, 15, 20, 30, 40, 50, 100, 300, 500 mJy/beam. The HPBW of the restoring beam is 1.00×0.86, p.a. −30°. **d** Epoch 1994.7. Peak flux is 626 mJy/beam. Levels are −3, 3, 5, 7, 10, 12, 15, 20, 30, 50, 100, 300, 500 mJy/beam. The HPBW of the restoring beam is 1.01×0.91, p.a. −25°.

Table 2. VLBI map parameters

4990.99 MHz

(1) Epoch	(2) Beam mas, ∘	(3) Noise mJy/beam	(4) S_{VLBI} mJy	(5) S_{core} mJy	(6) S_K mJy	(7) SNR
1986.4	1.16×0.67, −82	0.59	1547 ± 20	1159 ± 15	25 ± 3	1615
1988.2	1.16×0.67, −82	0.54	1503 ± 15	1121 ± 15	20 ± 3	1696
1992.2	1.00×0.86, −30	0.39	1267 ± 13	912 ± 10	66 ± 4	2144
1994.7	1.01×0.91, −25	0.52	1374± 14	634± 10	49± 5	1203

8416.99 MHz

1991.9	0.67×0.39, −14	0.34	1292 ± 13	1001 ± 10	61 ± 4	2589

Table 3. Component positions

Epoch	r, θ mas,°	r, θ mas,°	r, θ mas,°	r, θ mas,°	r, θ mas,°
1980.5	0.94±0.10, 196	2.30±0.10, 193	4.32±0.10, 195		
1983.9	1.41±0.10, 186	2.94±0.10, 191	5.68±0.10, 193		
1986.4	1.13±0.10, 182	2.59±0.10, 193	5.64±0.10, 193	6.76±0.20, 194	
1988.2	1.69±0.10, 182	3.03±0.10, 191	5.85±0.10, 194	8.56±0.20, 195	
1992.2	1.11±0.10, 189	3.27±0.10, 190	5.63±0.10, 191	9.74±0.20, 195	
1994.7	1.08±0.10, 214	4.12±0.10, 194	5.15±0.10, 194	6.25±0.10, 191	9.82±0.20, 195

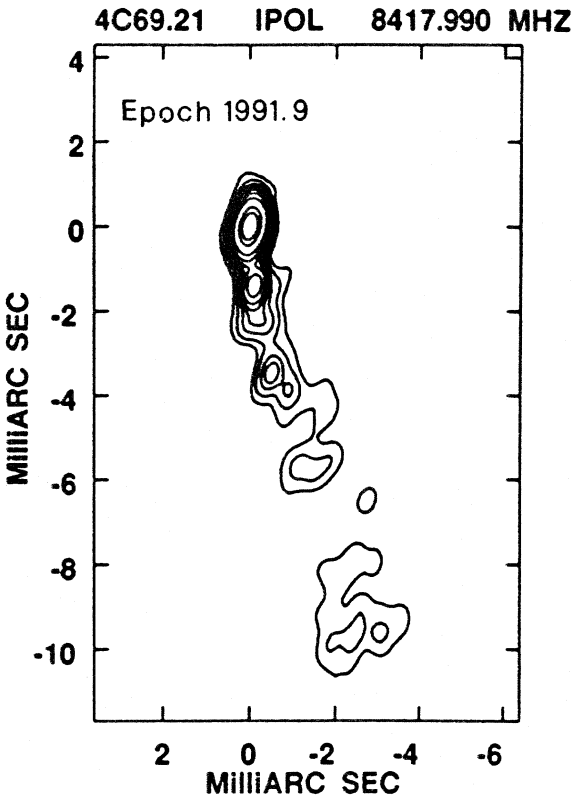

Fig. 2. Contour plots of the 3.6 cm map. The HPBW of the restoring beam is 0.67×0.39, p.a. −14°. The peak in the map is 880.3 mJy/beam, and the contour levels are −2, 2, 5, 10, 15, 20, 30, 50, 100, 300, 500 mJy/beam.

by roughly a factor of three (see maps shown in Figs. 1a–d and in Fig. 3).

In order to study the structural evolution of 1642+690, we have described the morphology of the source at each epoch using a few gaussian components derived by modelfitting the final visibilities of each dataset, and we have reported their positions in Table 3. This approach works well for the strongest components, i.e. those in the inner part of the structure (close to the core), but it becomes inadequate for the more complicated morphology of the jet beyond $\sim$ 4 mas from the core. This will be taken into account in the next section, where possible evolutionary scenarios for this source will be discussed.

We estimate that the error associated with the postion of each compact component is 0.10 mas, i.e. $\sim$ 10% of the beam, while for the extended ones we assume it to be $\sim$ 10% of the full width half maximum of the gaussian, as derived from modelfitting. We point out that a source of error in fitting the extended features is introduced by the fact that gaussian components could be inadequate representations of their morphology, so a more conservative estimate of the positional uncertainties is justified. The results are given in Table 3. Given the different appearance of the source from epoch to epoch, and in order to avoid a biased interpretation of the results, we have not labelled the various components in Table 3, and for each epoch we have simply given their position from the core. Labels will be given in Sect. 4, according to the scenario discussed.

As a cross check, we derived the distance between the barycenter of the southernmost component and the core from the numerical map made with AIPS at each epoch, and the value we

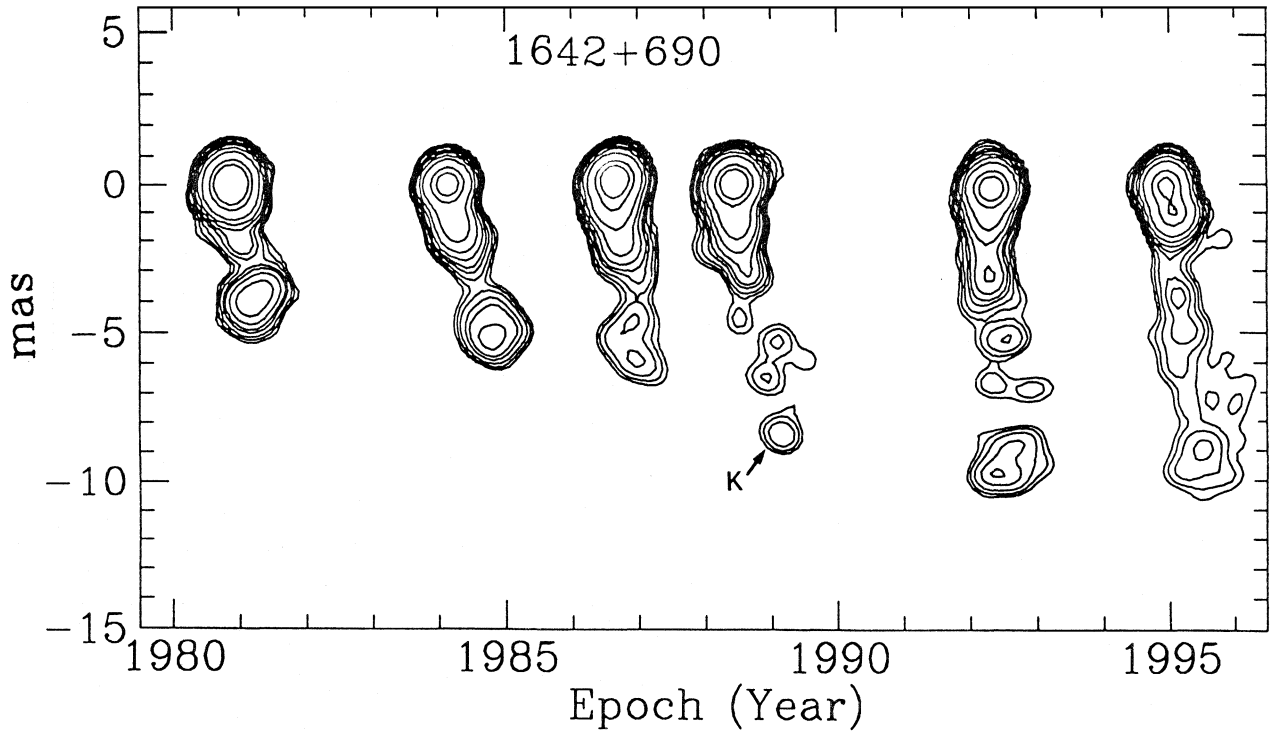

Fig. 3. Composite figure of the six epoch maps of 1642+690. All maps are convolved with a 1 mas circular beam. Contour levels are −5, 5, 7, 10, 15, 20, 30, 50, 100, 300, 500 mJy/beam in each map.

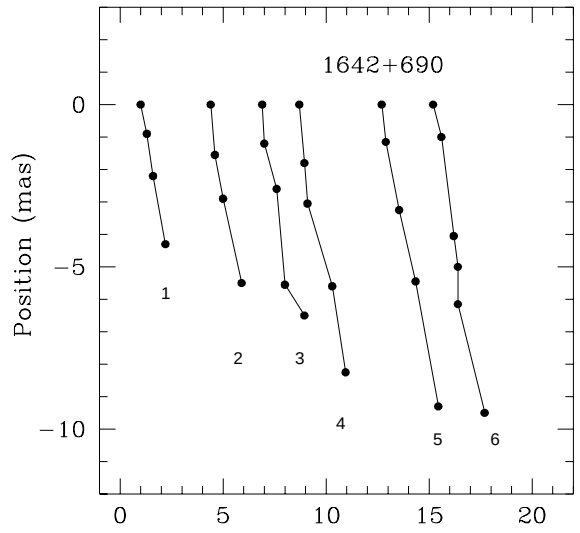

Fig. 4. Ridgeline of the peaks in the 6 cm maps at the six epochs. The separation of the ridgelines is proportional to the true separation in time of the epochs. The labels are as follows: 1 corresponds to epoch 1980.5, 2 to 1983.9, 3 to 1986.4, 4 to 1988.2, 5 to 1992.2, 6 to 1994.7.

derived is in very good agreement, within the estimated error, with the position obtained from the modelfitting.

In Fig. 4 we plot the ridgeline of the source, i.e. the positions of the peaks, on the plane of the sky at each epoch. The separation from epoch to epoch on the plot is proportional to the true separation in time.

3.2. The 3.6 cm map

The full resolution 3.6 cm map of 1642+69 (Fig. 2) and a lower resolution map, convolved with a circular beam of HPBW = 1.2 mas (not shown here) confirm the fact that the components along the jet do not follow a linear path.

The core is unresolved in the full resolution map. Using this map we made a gaussian fit to the dimension d of the jet in a direction perpendicular to that of propagation. The jet is is well collimated, with d ∼0.5 mas down to ∼4 mas from the core, then it widens up to a value of ∼1 mas at 6 mas at the expense of the surface brightness, which drops from 20 mJy/beam at the jet beginning, to 5 mJy/beam at 6 mas from the peak. Beyond this distance the jet is resolved roughly perpendicular to the direction of propagation. At this frequency the southernmost component shows an elongated morphology. A fit to its brightness distribution indicates that it can be resolved into two components, a compact and an extended one. The FWHM found with the program IMFIT in AIPS are 2.40×0.87 mas for the resolved one and 0.73×0.73 mas for the most compact. We derived the position of this component at the time of the 3.6 cm observations (1991.9) with respect to the peak in the map (coincident with the assumed stationary core) by modelfitting the final data set, and obtained a distance of 9.74 ± 0.15 mas, in p.a. 196°. This value is in good agreement with the positions derived from the fifth epoch 6 cm VLBI observations, taken four months later.

3.3. The VLBI spectrum

1642+690 is variable both at 6 cm and at 3.6 cm (Aller & Aller, private communication, see also the next paragraph), therefore

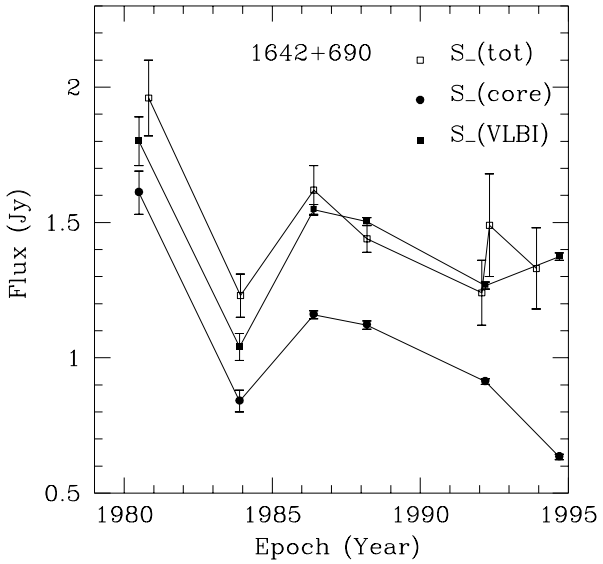

Fig. 5. Variations for the total flux density (open squares) (Aller & Aller, private communication), for the flux density measured in the VLBI maps (filled circles) and for the VLBI core flux density (filled squares) in in 1642+690 from 1980 to 1995.

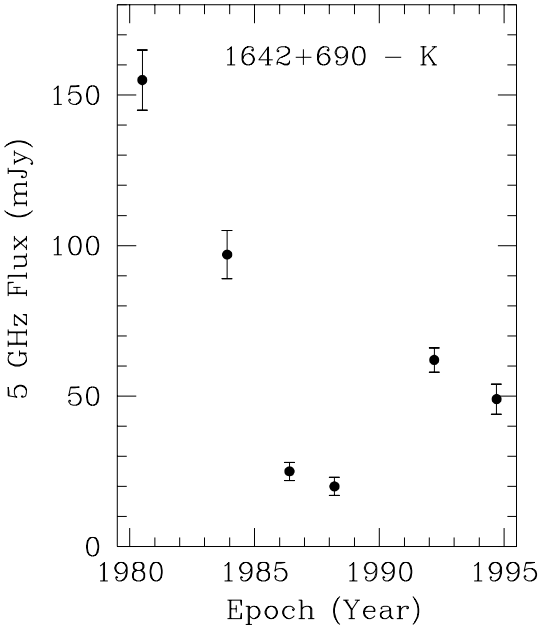

Fig. 6. Flux density of the southernmost component K at each epoch.

in order to derive the spectrum of the source simultaneous observations should be available. However the epoch of our 3.6 cm observations (1991.9) is only three months away from the fifth epoch of the 6 cm monitoring (1992.2), so we derived the spectral index for the source for epoch 1991.1. We estimated the 6 cm flux density of the strongest and most compact component in 1991.9 by interpolating its light curve at 6 cm as obtained from our set of observations, and obtained a value $S(6\,\mathrm{cm}) = 930 \pm 15$ mJy. The spectral index we derived is $\alpha_6^{3.6} = -0.14 \pm 0.05$. The compactness of this component, coupled with the shape of its spectrum in the range 3.6 cm - 6 cm, lead us to the conclusion that this is the core of the radio emission.

If we think that the VLBI 6 cm flux density variations are due mainly to flux changes in the core, as discussed in Sect. 3.4 and shown in Fig. 5, we can obtain a rough estimate of the spectral index along the jet, assuming that the 6 cm flux of 1642+690 along the jet did not change from 1991.9 to 1992. We find $\alpha_6^{3.6} \sim 0.5$ along the jet, then the spectrum of the southernmost knot flattens again and $\alpha_6^{3.6} \sim 0$.

3.4. Flux density variations

Another important piece of information on the morphological changes of 1642+690 comes from the flux density variations of the various components in the source.

The total 6 cm VLBI flux density of the source S_{VLBI} is variable. It had a maximum in 1980.5 ($S = 1937 \pm 20$ mJy), then it dropped down to 1235 ± 12 mJy in 1983.9 (Paper I). It had a secondary maximum in 1986.4 (see Table 2), decreased between 1986.4 and 1992.2 and increased less than 10% from the fifth to the sixth epoch. The largest fraction of the flux density changes in the VLBI morphology is due to variations in the core, as is clear from Table 2 and Fig. 5, where the single dish flux density of the source is also plotted (Aller & Aller, private communication).

From our maps it is clear that the flux density S of the southernmost component K varies with time, as shown in Table 2 and Fig. 6. It steadily increased from 1986.4 to 1992.2, then it dropped by about 20% from the fifth to the sixth epoch.

4. Discussion

The results of our monitoring program support the superluminal nature of 1642+690. However, the complicated morphological variations of 1642+690 during the 15 years of our monitoring do not allow an unambiguous and straightforward interpretation of the phenomena observed. In particular, the identification of components along the jet from one epoch to the other is not unique and alternative possibilities should be taken into account. In this Section we will consider two frameworks both for the first 6 mas of the jet and for the southernmost component, and will discuss possible evolutionary scenarios.

Throughout the discussion we will assume that bulk speed β_b and pattern speed β_p are the same. This assumption will allow us to derive information on the intrinsic plasma flow directly from the superluminal motion along the jet using the equation:

$$\beta_{\mathrm{app}} = \frac{\beta_p \sin\theta}{1 - \beta_p \cos\theta}$$

(Pearson & Zensus 1987).

The case $r \equiv \frac{\beta_p}{\beta_b} \neq 1$ is not ruled out (see Vermeulen & Cohen 1994, for a thorough discussion on the issue), but we will not discuss it in the present paper.

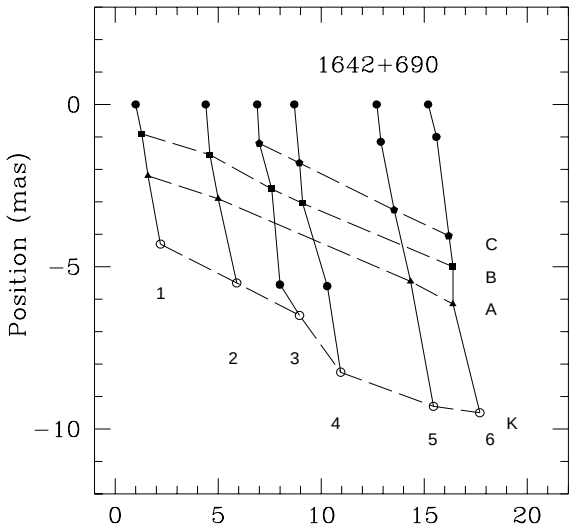

Fig. 7. Proposed evolution of components A, B and C in 1642+690. Component K is also indicated. Epochs are numbered as in Fig. 4.

4.1. Proper motion along the inner jet

One possible explanation for the morphological changes observed within the first 6 mas from the core of 1642+690 is illustrated in Fig. 7, where the same components at the various epochs have been represented with the same symbol. Lines indicating the proposed evolutionary sequence for the various components have also been drawn. We have labelled the southernmost component as K, and those along the jet from A to C starting from that further away from the core.

In this framework, components A and B have been visible in our maps since the first epoch, while component C has clearly emerged from the core in the third epoch. From the positions given in Table 3, we fitted the proper motion for each component, and the derived the corresponding apparent speeds:

$$\mu_A = 0.25 \pm 0.03 \text{ mas y}^{-1} \quad \beta_{\rm app}(A) = 6.8 \pm 0.8$$
$$\mu_B = 0.29 \pm 0.06 \text{ mas y}^{-1} \quad \beta_{\rm app}(B) = 7.9 \pm 1.6$$
$$\mu_C = 0.35 \pm 0.02 \text{ mas y}^{-1} \quad \beta_{\rm app}(C) = 9.6 \pm 0.5$$

The apparent speeds derived for components A and B agree, within the errors, while that of component C is marginally higher. In this framework 1642+690 would be characterised by a flow of superluminal components with very similar, high apparent speed. These velocities are in agreement with the superluminal apparent velocity, $\beta_{\rm app} = 9.3$, derived in Paper I for the southernmost component, labelled K in the present work. We point out that this apparent motion is among the highest ever detected (see Vermeulen & Cohen 1994, for a large database collection and a detailed discussion on this issue).

An apparent speed in the range $\beta_{\rm app} = 8 \div 9$ gives an intrinsic plasma speed $\beta_{\rm intr} \gtrsim 0.992 \div 0.994$, $\gamma_{\rm min} \gtrsim 8 \div 9$, and an orientation to the line of sight $\theta_{\rm min} \gtrsim 6^\circ \div 7^\circ$.

As stated above, component C emerged in 1986.4. Tracing back its evolutionary path, we can see that it was unresolved from the core in our 1983.9 observations and was coincident with the core itself around 1982. From Fig. 5 it is clear that the source flux density had a maximum in 1980.5, and a secondary peak around 1986. The superluminal component C could be associated with the burst of radio emission observed in the source around 1980.

Component B seems to be missing in the 1992.2 map. However, as stated in Sect. 3.1, our gaussian components could be an inadequate representation of the jet morphology, and we may have missed some critical features. In particular, both from Fig. 1c and Fig. 3, it is clear that a component is present southeast of component B, but blended with it in our maps. The same explanation could be given for the lack of component A in epochs 1986.4 and 1988.2.

Alternative identifications for the inner part of the jet lead to varying apparent speeds and paths for the various components. This has already been reported for 3C345 (Unwin & Wehrle 1992). In our case, however, the situation is complicated by the fact that we should also take into account superluminal contraction, as it is clear by inspection of the ridgelines in Fig. 4. If we exclude the possibility of component ejection and flow, and assume for example that the component closest to the core is the same one going from 1986.4 to 1994.7 then we must explain its superluminal contraction going from 1988.2 to 1992.2. The same is true for the second component along the jet.

An important issue is the major change of the nuclear region of 1642+690 between the last two epochs. The most compact feature in the 1992.2 map split into two components. Assuming that the core is the northernmost, most compact feature, its flux dropped considerably (see Table 2), and the flux of the secondary nuclear component is ~ 0.5 Jy. Furthermore the whole source structure within the first 1.5 mas from the peak has rotated by $\sim 16^\circ$ with respect to the previous epoch. This is quite interesting, since the overall alignment has been stable over the 15 years of our monitoring. One possibility is that we have been watching the ejection of another component, in a different position angle. The continuation of our monitoring program would be very helpful to support this hypothesis.

4.2. Evolution of the southernmost component

The location of the southernmost component K during the fifteen years of our monitoring program is the clearest evidence for the superluminal expansion of 1642+690, if we assume that we have been watching the same feature evolving over the time. However the interpretation of the evolution of K is not trivial. For the following discussion the southernmost component will be labelled as K in epoch 1988.2, 1992.2 and 1994.7, and as K′ in the three previous epochs. We will consider two possible cases, i.e. *(a)* K and K′ are the same feature; *(b)* K and K′ are two different components.

4.2.1. (a) K = K′. Bending and/or intrinsic changes

If K = K′, then the position, flux and morphology of this feature have changed a lot, the most dramatic change taking place from 1983.9 and 1986.4, when it split into two components. The morphology of this feature has been changing ever since, becoming

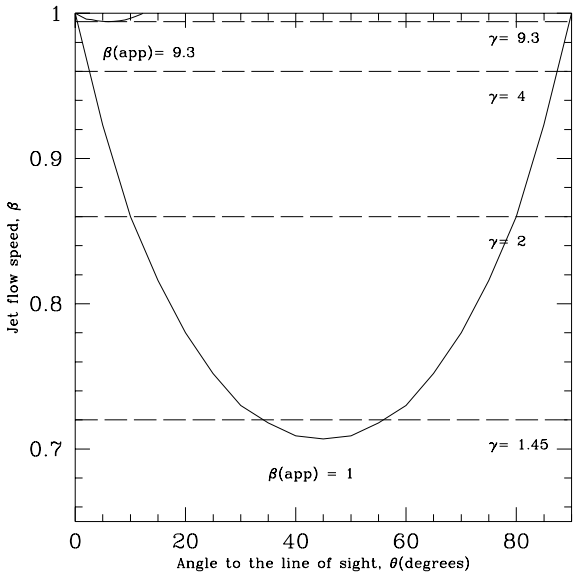

Fig. 8. Dependance of the apparent speed $\beta_{\rm app}$ (heavy lines) on the angle to the line of sight θ and the intrinsic flow speed $\beta_{\rm intr}$. Dotted lines represent the Lorentz factor γ corresponding to the values of β.

more diffuse and with a lower surface brightness from epoch to epoch (Fig. 3).

The models we derived by modelfitting the final dataset at each epoch indicate that this component is moving southwards with a complex kinematics. Fig. 7 shows that it is impossible to derive a single expansion velocity, even allowing for the uncertainties in its position at each epoch. Things are even more difficult to understand if we take into account the source morphology at the first two epochs. The position of K with respect to the core from 1980.3 to 1986.4 can be fitted very well with a single apparent expansion velocity of 9.3c, as given in Paper I, and in agreement with the apparent speed of the jet region closest to the core, as discussed in Sect. 4.1. This velocity however is inadequate to fit the data beyond epoch 1986.4. From Fig. 7 it is clear that K accelerated from 1986.4 to 1988.2, then it has been decelerating ever since, and has remained almost stationary within the errors from 1992.2 to 1994.7. Such behaviour is hard to explain with simple assumptions.

Changes in the apparent motion of superluminal components could be due to several causes.

Assuming that the core is stationary, and that $\beta_b = \beta_p$, they could be intrinsic, i.e due to changes in the intrinsic Lorentz factor γ, or could be due to geometrical effects, such as bending of the jet with respect to the line of sight, or a combination of both. If the initial assumption that the core is stationary does not hold, then the picture becomes even more complicated (Zensus et al. 1995). In Fig. 8 we have reported the dependance of the apparent speed on the angle to the line of sight and on the intrinsic plasma speed. The two curves correspond to $\beta_{\rm app} = 9.3$ and $\beta_{\rm app} = 1$ (a situation consistent, within the errors, with the position of component K in the last two epochs). From the figure we can derive the following considerations. If θ remained constant, γ changed by a large amount (from 9.3 to almost 2 if $\theta = \theta_{\rm min}$). Alternatively, if γ remained constant, then the jet has either bent towards the line of sight and is now almost aligned with it ($\theta \sim 0°$), or off the line of sight and is now almost in the plane of the sky.

None of these three possibilities is in agreement with the flux density changes observed for knot K in our 6 cm maps (see Table 2 and Fig. 6). The flux density of components depends on the Doppler factor with a law δ^η, where $\eta = 3 + \alpha \sim 3.5$ and $\delta = \gamma^{-1}(1 - \beta\cos\theta)^{-1}$. A major change in β at constant θ would imply a drop in δ from ~ 9 to ~ 3; keeping β constant and bending the jet towards the line of sight would increase δ by about a factor of 2; finally keeping β constant and bending the jet off the line of sight would decrease δ by almost two orders of magnitude. A simple frame seems therefore inadequate to explain the properties of component K.

4.2.2. (b) K $\neq$ K′. Flaring and expansion of a component

Another possibility is that K $\neq$ K′, and K is actually an "old", previously hidden component which is now expanding and evolving.

The flux density increase detected in K up to 1992.2 could indicate that the component was initially self-absorbed and it is now optically thin (see for example Kellermann & Pauliny-Toth, 1968, for a review of the theory of compact extragalactic radio sources). The flat spectrum between 6 cm and 3.6 cm (see Sect. 3.3) would be in agreement with the component becoming optically thin at 6 cm around 1992. This possibility does not seem very likely. First of all the flux density changes reported for K do not fully agree with the expected decrease for an expanding, optically thin component (Kellermann & Pauliny-Toth 1968). Furthermore, if this were the case, K′ should have been visible at higher frequencies. However no component is seen in 1642+690 either at 22 GHz (Wehrle, private communication) or at 10 GHz (Unwin, unpublished) beyond the first 2 mas from the core.

A more plausible alternative is that K′ has brightened as consequence of increased energy dissipation along the jet flowing out of the core.

In case component K in the last three epochs is actually an old hidden component, the evolution of K′ in the first three epochs remains an open question. If we connect K′ between 1980.5 and 1983.9 in Fig. 3 (not drawn here) and continue this line to epoch 1994.7, we connect peaks of components in each map. Such line could therefore represent an alternative evolutionary path for K′. In this frame the superluminal character of K′ would be confirmed, at the speed $\beta_{\rm app}$ derived in Paper I, i.e. $\beta_{\rm app} = 9.3$.

4.3. General comments

To summarise, it is difficult to discriminate among the possible frameworks given in the previous two paragraphs. Given the morphological and flux density changes of the source detected during our monitoring program, we favour the interpretation that 1642+690 is a superluminal radio loud quasar, characterised by

a flow of components ejected from the nucleus at high, $\beta_{\rm app} \sim 9$, almost equal speed. This can be explained in the standard Doppler boosting scenario assuming a high intrinsic plasma speed ($\beta_{\rm intr} \sim 0.994$) and a small angle between the velocity vector and the line of sight ($\theta \lesssim 12^\circ$). Our analysis does not supply strong evidence for major changes in the orientation of the velocity vector to the line of sight, either in the form of bending or of helical motion along the source jet.

The evolution of the southernmost knot remains a matter of concern. Bending and/or intrinsic changes in the Lorentz factor are not in agreement with the observed flux density changes, while brightening and expansion of a "hidden", self-absorbed component are not in agreement with the flux density changes and with the morphology of the source at higher frequencies. A possibility is that the southernmost knot has become visible as a consequence of increased energy dissipation.

It is worth commenting here on the lack of γ-ray emission from 1642+690. The high $\beta_{\rm app}$ proposed for this source makes it a candidate for γ-ray emission, but no emission was detected by EGRET (Fichtel et al., 1994). To explain the strong emission from blazars at high energies, Maraschi, Ghisellini & Celotti (1992) proposed that X- and γ-ray emission and synchrotron emission at lower frequencies are connected via inverse Compton scattering in a relativistic jet oriented close to the line of sight. For this reason, superluminal radio sources are the best candidates for γ-ray emission. However, even though all γ-loud quasars are characterised by superluminal motion on the parsec-scale, the opposite is not true, i.e., some superluminal blazars and flat-spectrum radio quasars are not γ-ray emitters (von Montigny et al., 1995). The lack of γ-ray emission from this subclass of superluminal sources was attributed by those authors to variability and/or orientation and geometry of the beamed γ-ray emission. The lack of γ-ray emission for 1642+690 therefore does not constitute a problem, despite the high apparent speed claimed in Paper I and in the present work, and such behaviour is shared by other superluminal radio sources.

Acknowledgements. We are grateful to the U.S. and European VLBI Networks for allocating all the observing time necessary to carry out our monitoring program. We thank G.B. Taylor and R.C. Vermeulen for their help in the scheduling and data reduction of the 1994.7 observations. Thanks are due to Margo and Hugh Aller for providing the data of their monitoring program in advance of publication.

References

Conway, J.E., Murphy, D.W., 1993, ApJ, 411, 89
Fichtel, C.E., Bertsch, D.L., Chiang, J., Dingus, B.L., Esposito, J.A., Fierro, J.M., Hartman, R.C., Hunter, S.D., Kanbach, G., et al., 1994, ApJS, 94, 551
Kellermann, K.I., Pauliny-Toth, I.I.K, 1968, ARAA, 6, 417
Maraschi, L., Ghisellini, G., Celotti, A., 1992, ApJ, 397, L5
Murphy, D.W., Browne, I., Perley, R.A., 1993, MNRAS, 264, 298
O'Dea, C.P., Barvainis, R., Challis, P.M., 1988, AJ, 96, 2
Pearson, T.J., 1991, BAAS, 23,991
Pearson, T.J., Readhead, A.C.S., 1988, ApJ, 328, 114
Pearson, T.J., Zensus, A., 1987, in Superluminal Radio Sources, ed. A. Zensus & T.J. Pearson (Cambridge: Cambridge University Press), 1
Pearson, T.J., Barthel, P.D., Lawrence, C.R., Readhead, A.C.S., 1986, ApJ, 300, L25 (Paper I)
Polatidis, A.G., Wilkinson, P.N., Xu, W., Readhead, A.C.S., Pearson, T.J., Taylor, G.B., Vermeulen, R.C., 1995, ApJS, 98, 1
Scheuer, P.A.G & Readhead, A.C.S., 1979, Nature, 277, 182
Schwab, F.R. & Cotton, W.D., 1983, AJ, 88, 688
Shepherd, M.C., Pearson, T.J., Taylor, G.B., 1994, BAAS, 26, 987
Taylor, G.B., Vermeulen, R.C., Pearson, T.J., Readhead, A.C.S., Henstock, D.R., Browne, I.W.A., Wilkinson, P.N., 1994, ApJSS, 95, 345
Unwin, S.C., Wehrle, A.E., 1992, ApJ, 398, 74
Vermeulen, R.C., Cohen, M.H., 1994, ApJ, 430, 467
von Montigny C. et al., 1995, A&A, 299, 680
Wrobel, J.M., 1993, AJ, 106, 444
Zensus, J.A., Cohen M.H., Unwin, S.C., 1995, ApJ, 443, 35
Zensus, J.A., Krichbaum, P.T., Lobanov, A.P., 1995, Proc. Natl. Acad. Sci., Vol. 92, p. 11348

This article was processed by the author using Springer-Verlag LaTeX A&A style file *L-AA* version 3.